Applied Energy 312 (2022) 118700

Contents lists available at ScienceDirect

Applied Energy

journal homepage: www.elsevier.com/locate/apenergy

Operation and performance of Brayton Pumped Thermal Energy Storage with additional latent storage

Max Albert, Zhiwei Ma *, Huashan Bao, Anthony Paul Roskilly

Department of Engineering, Durham University, Durham, UK

ARTICLE INFO

Keywords:
Pumped Thermal Energy Storage
Round-trip efficiency
Phase Change Material
Power front
Schumann model

ABSTRACT

Pumped Thermal Energy Storage (PTES) is an increasingly attractive area of research due to its multidimensional advantages over other grid scale electricity storage technologies. This paper built a model and numerically studied the performance of an Argon based Brayton type PTES system. The model was used to optimise total work output and round-trip efficiency of the system. The aspect ratio of the thermal storage tanks and operation of packed bed segmentation have been varied to assess their impacts on round-trip efficiency. Longer and thinner tanks were found to increase efficiency, with the hot tank length affecting system performance to a greater extent than the cold tank. Larger 'temperature ratio' in segmentation operation were found to develop higher round-trip efficiency, with higher exit working fluid temperature from hot storage over a shorter duration demonstrating better performance. Key features describing the power output were identified as the duration of the region of maximum power and the steepness of the 'power front'. To maximise the duration of the high power region and decrease the width of the power front, additional latent heat storage was used, the effect of which on round-trip efficiency was then assessed with predicted efficiencies of up to 80% using isentropic reciprocating compressor/expander architecture, which is close to the theoretically predicted limit.

1. Introduction

The United Nations state that access to affordable and clean energy is vital in establishing a sustainable and equitable society [1]. Meeting the needs of a developing global grid will be key if this goal is to be achieved. However, the race to net-zero is collecting a global collateral of intermittent renewable energy generation sources with the global proportion of electricity generated by these Renewable Energy Sources (RES) topping 25% in 2020 [2]. As conventional (fossil and nuclear) power stations are phased out of the energy mix, the reliability and flexibility of power generation is being called into question [3].

The intermittent issue of solar energy, geographical constraints of hydro-generation, and limitations of frequency control in early wind turbines has added complexity to the global renewable drive [3]. Storing energy as gravitational, kinetic, electric or thermal potential allows each of the issues identified with RES to be addressed and mitigated [3]. Such Energy Storage Systems (ESS) are described by the World Energy Council as the 'Critical missing link between intermittent renewable power and a 24/7 reliability net-zero carbon scenario' [4]. ESS have the potential for financial as well as grid reliability benefits. Energy consumed to charge the storage when electricity prices are low, can be released at peak cost times for profit in a system known as '*arbitrage*'. Dunbar et al. [5] identified the evolution that this market would undergo as energy pricing shifts from conventional to renewable fuels with the potential for falling electricity costs. However, the use of ESS to spontaneously increase power supply to meet peak demand and time shift distribution must be considered within a wider practical framework [6].

Gallo et al. [3] highlighted Pumped Hydroelectric Storage (PHS), Battery technology and Compressed Air Energy Storage Systems (CAES) as the only technologies to have demonstrated a sufficient maturity to be commercially viable. They can achieve round-trip efficiency at 65%–87%, 85%–90%, and 50%–89% respectively [7]. Among these three technologies, PHS has been most commonly adopted with over 96% of installed ESS developed in PHS [2]. However, the ecological damage caused by the flooding of valleys and the 100 m height requirement are limiting the attraction of future expansion.

Comparing to other grid scale electricity storage technologies, Pumped Thermal Energy Storage (PTES) has been believed to have relatively high energy storage density and low installation capital cost, it has no geographical limitation or output power limitation. Three camps of PTES technology are widely acknowledged, these utilise Rankine, Brayton, and Transcritical cycles. At energy charge stage,

* Corresponding author.
E-mail address: zhiwei.ma@durham.ac.uk (Z. Ma).

https://doi.org/10.1016/j.apenergy.2022.118700
Received 13 July 2021; Received in revised form 15 January 2022; Accepted 6 February 2022
Available online 26 February 2022
0306-2619/

Nomenclature

Latin

A	Cross-sectional area, (m^2)
A_t	Yearly system cost, (€)
c	Specific heat capacity, (kJ/kg K)
$CPEX$	Capital expenditure, (€/kW or €/kWh)
d_p	Particle diameter, (m)
h	Heat transfer coefficient, (W/m^2 K)
ΔH	Specific latent heat, (kJ/kg)
k	Thermal conductivity, (W/m K)
L_{eff}	Effective length, (m)
$\dot{m}$	Mass flow rate, (kg/s)
M	Mass, (kg)
$OPEX$	Operating expenditure, (€/kW or €/kWh)
ΔP	Pressure drop, (Pa)
P_{peak}	Peak power during discharge, (kW)
PR	Pressure ratio, (–)
Pr	Prandtl number, (–)
$\dot{Q}$	Heat transfer rate, (kW)
Re	Reynold number, (–)
S_v	Surface area to volume ratio, (m^2/m^3)
t_{pm}	Duration of maximum power output, (h)
T	Temperature, (K or °C)
T_{melt}	Melting temperature of the PCM, (°C)
u_g	Gas velocity, (m/s)
w	Work or specific work, (kJ or kJ/kg)

Greek

γ	Ratio of specific heats, C_p/C_v (–)
ε	Void fraction (–)
η	Efficiency, (–)
ρ	Density, (kg/m^3)

Subscripts

cond, conv	Heat transfer mode: conduction/convection
chg,dis	System process: charge/discharge
exit	Gas condition at exit
g,l,s	Material phase: solid/ liquid/gas
rt	Round-trip
1,2,3,4	Property at state

Abbreviations

B-PTES	Brayton-PTES system
CAES	Compressed Air Energy Storage
CE	Compressor–Expander
ESS	Energy Storage Systems
PCM	Phase Change Material
PHS	Pumped Hydroelectric Storage
PTES	Pumped Thermal Energy Storage
RES	Renewable Energy Sources
TES	Thermal Energy Storage

the working fluid of Rankine PTES is condensed to liquid in the hot storage and evaporated to vapour in the cold storage; the working fluid maintains at vapour phase through the whole Brayton PTES cycle; and in Transcritical PTES, the working fluid is at vapour phase in hot storage and at liquid phase when enters cold storage then evaporates to vapour. Besides many academic researches, several commercial PTES systems have been developed (or under development) including Malta's Rankine PTES [8], Isentropic's Brayton PTES [9], and MAN Energy Solutions's transcritical PTES [10]. However, current research and development are still at early stage, some controversial results on the key performance indicator (round-trip efficiency) have been reported; the impact of thermal energy storage on the system performance has not been fully explored; studies on how to realise the maximum potential of PTES in practice are urgently needed.

For Brayton PTES, which is the focus of this study, McTigue [11] conducted an exergy or availability analysis to develop the upper limit of round-trip efficiency while not violating thermodynamic laws. This was built on second law analyses of the irreversibility generated from the heat transfer of the working fluid with the storage medium as well as losses from the Compressor and Expander (CE) devices and heat exchangers. It suggested Brayton PTES systems could achieve round-trip efficiencies between 40%–80%. White et al. [12] thermodynamically analysed the round-trip efficiency of Brayton PTES system and found that the round-trip efficiency was sensitive to the compression and expansion irreversibility. Further study by the same group of researchers [13] suggested a round-trip efficiency near 70% with the consideration of the mechanical and electrical losses of reciprocating type compressor and expander, however, if turbomachinery was used the system round-trip efficiency was unlikely to exceed 50%. Nevertheless, numerical analysis by Benato [14] suggested a low round-trip efficiency at around 10%, mainly contributed to the non-isentropic processes of compression and expansion as well as the large thermocline in hot and cold stores. Further study by Benato and Stoppato [15] suggested shortening the charging time in order to minimise heat rejection to the environment and maximise round-trip efficiency.

Some researches have been conducted into the effect of Thermal Energy Storage (TES) performance on the PTES system. The most common TES for Brayton PTES is the packed bed storage, which uses layers of gravel or other ceramic media inside insulated tanks. The integration of the storage media directly into the working fluid stream leads to good heat transfer and allows the entire system to operate at a single pressure. Practical care needs to be taken to avoid debris and smaller pebbles damaging the CE machinery [16]. White et al. [17] optimised the TES geometry looking to minimise losses from TES, considering both of reducing pressure losses of working fluid and increasing heat transfer area between working fluid and storage material. McTigue and White [18] used segmented packed bed aiming to reduce the thermal mixing losses. Laughlin [16] and Farres-Antunez et al. [19] employed split storage tanks and heat exchanger to improve heat transfer but at the increased expense of greater infrastructure.

The present study assessed and upgraded the performance of a Brayton PTES cycle with packed bed thermal energy storage, based on the system demonstrated by Isentropic Inc., UK, operating at a pressure ratio of 1:10 [20]. To develop an optimised system for the required storage application, the current paper modelled the instantaneous power output from this Brayton PTES system as the hot and cold thermal energy stores were discharged after a charge process. This study focused on the impact of thermal energy storage on PTES performance. Inspired by a packed bed storage study [21], the current study added latent heat storage at the downstream of sensible heat storage, which was found significantly effective on elongating the duration of power output at its maximum value and promoting the round-trip efficiency of PTES system.

2. Pumped thermal energy storage

Pumped Thermal Energy Storage is an ESS technology proposed in the 1920s when the term arbitrage was beginning to find meaning in

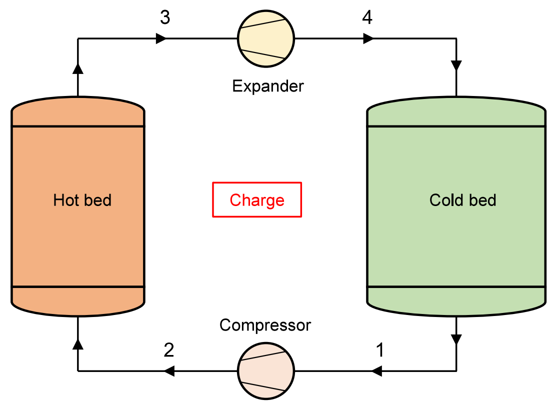

Fig. 1. Schematic diagram of an ideal B-PTES system.

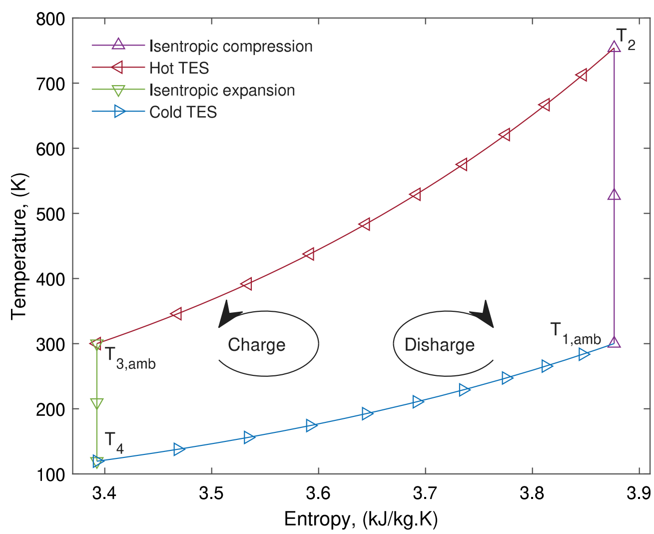

Fig. 2. Operational T-s diagram of an ideal Argon B-PTES system, operating from ambient conditions with a pressure ratio of 10:1. Full system schematics and technical and economic discussions of key components can be found in Ref. [11,12,20,22].

the context of an expanding power grid. Thermal energy storage in this form is geographically unconstrained and has the potential to store large quantities of energy near to generation sites or regions of high demand [11].

2.1. Cycle operation

The operation of PTES is divided into two phases, charge and discharge. The charge phase outlined in Figs. 1 and 2 uses electricity to drive a compressor, pressurising a working fluid and instilling it with thermal energy. Theoretically, in an ideal system, the hot working fluid passes through the hot store, heating the storage medium to the compressor outlet temperature, T_2. And the temperature of the working fluid returns to ambient, T_3, as the gas exits the hot store having given up its sensible heat to the storage medium. This high pressure gas flows through an expander to expand to a low pressure and reduce its temperature to T_4. This cold gas flows through the cold store back to the initial conditions at state 1.

The direction of the working fluid is reversed during discharge with the temperature difference at the exit of the hot and cold stores driving the expander and compressor and generating power. Real systems often employ recuperators or heat exchangers to vent any residual heat at the thermal store exit [11]. The compressor and expander run from the same shaft and so the duration of each phase is equal for heat and cold storage.

The system operates as a heat pump cycle during charge followed by a heat engine during discharge. The round-trip efficiency, η_{rt}, can therefore be expressed as:

$$\eta_{rt} = \eta_{HP} COP_{HE} = \frac{T_h - T_c}{T_h} \times \frac{T_h}{T_h - T_c} \tag{1}$$

The theoretical η_{rt} demonstrated by Eq. (1) predicts a system with 100% efficiency when operating between cycle limits ($T_h = T_2 \& T_C = T_4$ as shown in Fig. 2). This ideal result assumes perfectly efficient CE devices and perfect storage. In reality, the CE architecture is not ideal and losses can be attributed to the path function (polytropic losses) and frictional-heat losses. The effect of polytropic losses and thermal dissipation and mixing in the CE have been discussed in detail by White et al. [12].

2.2. PTES thermodynamics

Thermal energy is transferred to the working fluid during compression and expansion. The temperature increase across a device from inlet state 1 to outlet state 2 can be expressed in terms of the pressure ratio ($PR = \frac{P_2}{P_1}$):

$$\frac{T_2}{T_1} = PR^{\frac{\gamma-1}{\gamma}} \tag{2}$$

where γ is the polytropic index of the working fluid in the compression/expansion process, and equals to adiabatic index for an isentropic process.

The net specific work required to drive the pressure changes around the cycle can be expressed in terms of the state temperatures shown in Fig. 2:

$$w_{chg} = w_C - w_E = c_g(T_2 - T_1) - c_g(T_3 - T_4) \tag{3}$$

with similar equations for discharge work, w_{dis} [12]. In order to quantify the performance of a system, w_{dis} is commonly normalised by the energy consumption for charging, w_{chg}, and expressed as *round-trip efficiency*, η_{rt}.

This paper considers a Brayton PTES system built with a reciprocating type CE with an isentropic efficiency suggested by White et al. of 97.5% [12]. The use of reciprocating devices minimises the number of CE components and therefore system cost due to the potential for reversible operation. Therefore, the efficiencies of the CE devices are equal, $\eta_C = \eta_E = \eta_{CE}$ and the theoretical isentropic η_{rt} can be expressed in terms of ratio of work, $\frac{w_{dis}}{w_{chg}}$ [12]:

$$\eta_{rt} = \frac{\dot{m}_{dis} t_{dis} [c_g(T_2 - T_1)\eta_{CE} - c_g(T_3 - T_4)/\eta_{CE}]}{\dot{m}_{chg} t_{chg} [c_g(T_2 - T_1)/\eta_{CE} - c_g(T_3 - T_4)\eta_{CE}]} \tag{4}$$

where $c_g \times \Delta T$ equals the specific enthalpy at each state. This efficiency serves as a demonstrative upper limit for system performance considering only losses caused by non-isentropic CE processes.

2.3. Storage material

Sensible packed bed storage normally uses low-cost solid storage material, e.g., layers of gravel or ceramic material contained within insulated tanks, often under pressurisation. The direct contact of storage material and working fluid leads to large heat transfer area and high heat transfer performance, and also avoidance of the cost of additional heat exchanger and associated losses [11]. The practical limits of a sensible PTES system were assessed by Gallo et al. [3] who recommended sensible storage systems with power ratings from 0.001 to 10 MW for a capital cost of 3400–4500 $/kW. Furthermore, the Life Cycle Analysis carried out by Oró et al. [23] found sensible storage to have the lowest environmental impact per kWh compared to molten salt and PCM storage. Their findings specifically highlighted the proportion of impact caused by the containment and processing of high temperature systems such as molten salts.

Magnetite has been selected for the current analysis due to its high specific heat, mirroring the Isentropic Inc. demonstration system [22]. Magnetite was also reported with another attractive feature of PTES - high energy density by McTigue [11] suggesting a one-hundred fold improvement of PTES ($\rho_E = 100\ \mathrm{kWh/m^3}$) over PHS ($\rho_E = 1\ \mathrm{kWh/m^3}$). To aid the progression of the thermal front and reduce buoyancy driven mixing and hence irreversibility generation, the working fluid enters from the bottom of the hot/cold store when releasing heat to the storage material and enters from the top of store when absorbing heat from the storage material.

This study considered the performance of non-ideal thermal storage under a range of design conditions and analyse the effect on system efficiency.

2.4. Economic validation

Common methods of assessing the financial viability of an ESS include: analysing whether an investors money is worth spending on a proposed service or investing in the market, known as Net Present Value (NPV); the time required to recover the Capital expenditure, known as Payback period; and the total cost of the system normalised against the total energy it stores over its working life, or Levelised Cost of Storage (LCOS). Due to the uncertainty and complexity surrounding arbitrage pricing strategies coupled with the desire for cost comparison against other potential ESSs, NPV and payback periods were not considered within the scope of this work and a simple LCOS model has been constructed for the specified system operating three daily charge–discharge cycles [5,22]. The LCOS considers a full balanced plant from energy input to energy output including system components as detailed in [22]. It will be compared against existing ESS such as PHS which reported a LCOS between 0.13–0.17 €/kWh at 2016 prices [24].

3. Methodology

The following section details the model used to simulate the packed bed stores and assess the effect of geometry, segmentation and additional latent storage on the performance of PTES system, and the calculation of LCOS.

The packed beds are modelled as well-insulated tanks storing thermal material without heat leakage. During the charge cycle, the inlet gas temperature is equal to the CE exit temperatures. Using adiabatic inlet and outlet conditions the stores are discretized into N layers, as shown in Fig. 3. In all simulations of the sensible storage, N = 100 layers giving a trade off between performance and computation time. The percentage difference in reported η_{rt} using N = 100 & N = 200 is smaller than 1% validating this assumption. Based on the recommendations of White et al. [25] magnetite is used as the sensible medium with thermal properties obtained from Ref. [26], as presented in Table 1.

Heat transfer models of the packed bed storage and working fluid have been developed.

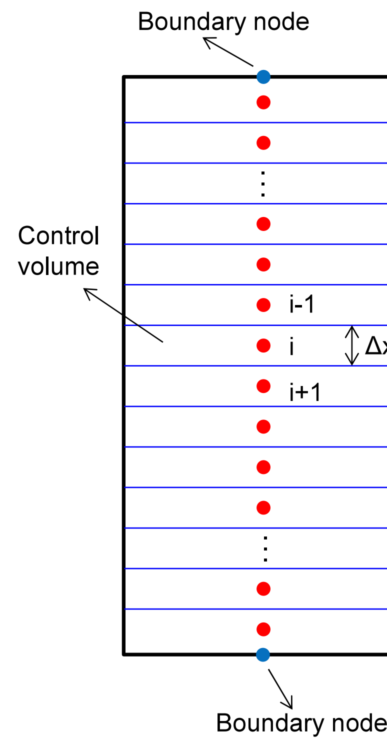

Fig. 3. Physical model of the packed bed used in the simulation process.

3.1. Packed bed assumptions

- Heat transfer occurs based only on the temperature difference between the solid and the gas, and by conduction along the solid layers. Conduction within the gas and heat leakage to the environment are considered small enough to be neglected.
- Heat transfer occurs axially along each packed bed neglecting radial variation.
- Unsteady gas terms are small and can be neglected: ($\Delta\rho_g \approx$ negligible and $\dot{m} \approx$ constant [11]).
- Gas properties: ρ_g, k_g, Prandtl number (Pr), & viscosity (μ_g) are calculated from the *CoolProp* library [27] and solid properties taken from available literature. Both will update as temperature varies throughout the simulation.
- The effect of radiation at the range of temperatures the system experiences is insignificant [12].
- Within each layer the particle size and conduction is small enough to consider the layer at a uniform temperature.
- Thermal and fluid boundary effects approaching the walls are neglected.
- Latent heat storage uses encapsulated PCM particles, the heat convection of liquid PCM is negligible.
- The thin encapsulation shell has no affect on the heat transfer, storage density and cost.
- Following the work of Wang et al. [28], the diameter of the particles in both the sensible and encapsulated PCM storage is 20 mm. The void fraction $\varepsilon = 0.3$.

Further implications of these assumptions are discussed by McTigue in [11].

3.2. First law energy balance equations

The rate of heat transfer within the solid can be expressed as sum of Newton's and Fourier's laws: $\dot{Q}_s = \dot{Q}_{conv} + \dot{Q}_{cond}$ where heat transfer

Table 1
Properties of the magnetite.

d_p, (mm)	20
ρ, (kg/m^3)	5173
c, (J/kg K)	$608.91893 + 1.42464T - 0.00151T^2 - 3.88207 \times 10^{-6}T^3 + 1.03616 \times 10^{-8}T^4$
k, (W/m K)	$6.22032 - 0.00485T - 6.04109 \times 10^{-6}T^2 + 9.60204 \times 10^{-9}T^3$

T has unit of °C

due to conduction entering (in) or leaving (out) each solid layer is proportional to $dT_s^{in/out}$:

$$M_s c_s \frac{dT_s}{dt} = hS_v(1-\varepsilon)A(T_g - T_s)dx + k_s A\left(\frac{dT_s^{in} - dT_s^{out}}{dx}\right) \tag{5}$$

leading to a rate of temperature change within the solid:

$$\frac{dT_s}{dt} = \frac{hS_v}{\rho_s c_s}(T_g - T_s) + \frac{k_s}{\rho_s c_s(1-\varepsilon)dx}\left(\frac{dT_s^{in} - dT_s^{out}}{dx}\right) \tag{6}$$

Heat transfer within the gas is assumed to occur solely by convection. Thus, considering energy changes within the gas:

$$A\varepsilon\rho_g c_g \frac{dT_g}{dt} + \dot{m}c_g\frac{dT_g}{dx} = hS_v(1-\varepsilon)A(T_s - T_g) \tag{7}$$

and by neglecting unsteady gas terms as discussed in [11], the temperature change along each packed bed is:

$$\frac{dT_g}{dx} = \frac{hS_v(1-\varepsilon)A}{\dot{m}c_g}(T_s - T_g) \tag{8}$$

The convection heat transfer coefficient between solid and gas in a packed bed, h, can be determined by the correlation established experimentally by Wakao et al. [29]:

$$h = \frac{k_g}{L_{eff}}(2 + 1.1Pr^{1/3}Re^{3/5}) \tag{9}$$

where the effective length, L_{eff}, is the particle diameter, d_p. k_g is the thermal conductivity of gas.

The above equations were solved using a semi-implicit numerical method for each control volume (layer i) shown in Fig. 3 with time step of 1 s. It is computed taking the average temperature between steps in space, $T^A = \frac{1}{2}(T_{i-1}^t + T_i^t)$, and time $T^B = \frac{1}{2}(T_i^t + T_i^{t-1})$ to improve accuracy.

For the gas:

$$\frac{T_{g,i}^t - T_{g,i-1}^t}{\Delta x} = \frac{hS_v(1-\varepsilon)A}{\dot{m}c_g}(T_s^A - T_g^A) \tag{10}$$

and the solid:

$$\frac{T_{s,i}^t - T_{s,i}^{t-1}}{\Delta t} = \frac{hS_v}{\rho_s c_s}(T_g^B - T_s^B) + \frac{k_s}{\rho_s c_s(1-\varepsilon)}\left(\frac{T_{s,i+1}^{t-1} - 2T_{s,i}^{t-1} + T_{s,i-1}^{t-1}}{\Delta x^2}\right) \tag{11}$$

The pressure drop, ΔP, along the packed bed is calculated for each layer of length, Δx, using the pressure loss equation developed by Ergun et al. [30]:

$$\frac{\Delta P}{\Delta x} = \frac{150\mu_g(1-\varepsilon)^2 u_g}{\varepsilon^3 d_p^2} + \frac{1.75(1-\varepsilon)\rho_g u_g^2}{\varepsilon^3 d_p} \tag{12}$$

where u_g is the gas velocity through the tank, μ_g is the gas viscosity. Gas pressure is updated and used to calculate the fluid properties for each layer as the simulation progresses.

3.3. Thermal storage tank volume

While charging, the work done by the system is in equilibrium, $Q_{hot} + w_E = Q_{cold} + w_C$. For the charging power and time specified, the energy stored in the tanks can be calculated. Use of Eq. (13) to find the mass, M, in combination with the solid density and tank void fraction allows the required tank volumes, ($V^{hot/cold}$), to be sized.

$$w_C - w_E = Q_{hot} - Q_{cold} = M^{hot}c_s^{hot}(T_2 - T_3) - M^{cold}c_s^{cold}(T_1 - T_4) \tag{13}$$

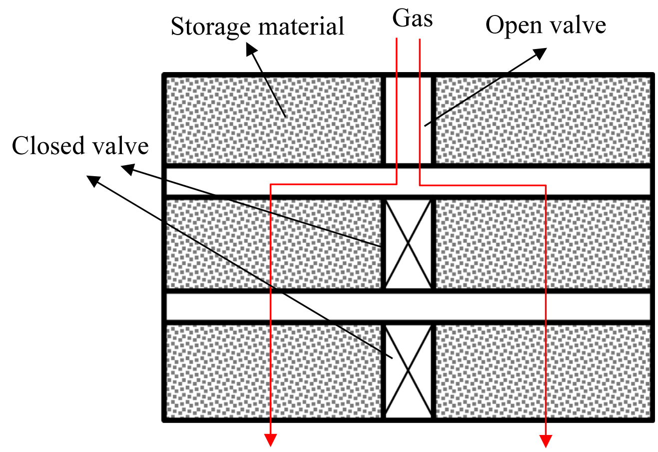

Fig. 4. Physical model of the packed bed used in the simulation process.

3.4. Segmentation operation

Segmented storage was assessed with the aim of reducing pressure losses and improving round-trip efficiency of the whole system by stabilising the outlet temperature of working fluid from hot and cold stores. The operation of the segmentation has been modelled [31], patented and demonstrated by Isentropic Inc.

The proposed thermal storage tank incorporates a bypass flow route past each storage layer. By blocking the bypass channel for a specific layer the working fluid is forced through the path of least resistance, in this case the packed storage material, as illustrated in Fig. 4. Once the outlet layer (final active layer) storage material reaches a desired fraction of the storage temperature - 'temperature fraction' (T_{outlet}/T_{store}), the bypass route is opened and the path of least resistance becomes the bypass channel, and storage material in other layers becomes active.

In current study, initially the first three bypass paths would be blocked forcing the fluid through these storage material. Exiting the third layer, the flow will then follow the path through the open bypass channels to the storage exit. Once the solid in the third layer has reached a specified percentage of the storage temperature (temperature fraction), the first layer is bypassed and the fourth layer will be activated. As successive layers reach the desired temperature, the sequence of opening and closing off layers rolls on until the entire thermal storage reaches the desired temperature.

3.5. Latent heat transfer

Heat transfer between encapsulated PCM with a particle diameter of 20 mm and the working fluid is consistent with the relations and numerical method developed in Eqs. (6) & (11).

The heat stored in the PCM is the sum of the energy due to sensible temperature change and the latent heat, ΔH:

$$\Delta Q = Mc_{PCM,s}(T_{melt} - T_{initial}) + M\Delta H + Mc_{PCM,l}(T_{end} - T_{melt}) \tag{14}$$

The phase change was modelled at constant temperature. In the phase change region, the heat transfer calculated by the left side of Eq. (5) is added to the latent energy. Once the accumulated latent energy is larger than the latent heat of the used PCM, the material then

Table 2
Properties of the PCMs trialled as latent storage.

	Zinc		KNO_3		$NaNO_3$		E-78		E-114	
	s	l	s	l	s	l	s	l	s	l
ρ, (kg/m^3)	7140	6570	1900	1890	2261	1900	880		782	
c, (J/kg K)	390	480	920	1220	1080	1830	1960		2390	
k, (W/m K)	108	51	0.69	0.39	0.80	0.50	0.54		0.54	
ΔH, (kJ/kg)	112		266		172		115		107	
T_{melt}, (°C)	419		333		307		−78		−114	

exits phase change region to liquid state in heating process or solid state in cooling process.

The PCMs analysed in the hot store include *Zinc* with properties taken from [32,33], KNO_3 [34–36] & $NaNO_3$ [34–36]. In the cold store, eutectic ultra-low temperature PCMs, *E-78* [37] & *E-114* [37] were used. These PCMs are assumed to be ideal neglecting hysteresis and sub-cooling. Data for the liquid phase of cold PCMs were unavailable and so solid properties were used in all regions. PCM properties are shown in Table 2.

3.6. Power output

Following the recommendation of Schoenung [38] and Wang et al. [28], a symmetric charge–discharge cycle of four hours is proposed to address the mismatch between energy supply and demand in a day. The PTES system in this study has been designed to have a nominal power of 1 MW therefore to store 4 MWh of energy in a system.

The discharge power and time of discharge were used as conditions for the termination of the simulation. The discharge power was calculated as the product of the net work output and the mass flow rate:

$$P_{dis} = \dot{m}_{dis}[\eta_{CE}(h_2 - h_1) - (h_3 - h_4)/\eta_{CE}] \tag{15}$$

and integrated using a simple Simpson's rule to find the total work output and hence the efficiency $\eta_{rt} = w_{dis}/w_{chg}$.

Each simulation was terminated when $P_{dis} \leq 0$ or $t_{dis} = 4$ h.

3.7. LCOS

The cost to run the system for a given year, A_t, is the sum of the operating costs, $OPEX_t$ (€/kW & €/kWh), and the cost of electricity, c_{el} (€), shown in Eq. (16) for that year. This is discounted at a rate of i%. The cost of maintenance is accounted for with a reinvestment factor, $CAPEX_{re}$ (€), and the residual value of components at the end of the system lifetime is expressed as R (€).

$$A_t = OPEX_t + CAPEX_{re,t} + c_{el} \cdot w_{chg} - R_t \tag{16}$$

The lifetime system cost can be calculated by adding the capital expenditure, $CAPEX$ (€/kW & €/kWh), to the cumulative yearly system cost, A_t (€). The yearly system cost is summed over the system lifetime, n, to obtain the total operational costs. The residual value of components over a 20 year life time, and estimates of the cost of maintenance lie beyond the scope of the current work ($R = CAPEX_{re} = 0$). Further details on the method can be found in Ref. [22]. Then, the Levelized Cost of Storage (LOCS) is expressed in Eq. (17).

$$LCOS = \frac{CAPEX + \sum_{t=1}^{t=n} \frac{A_t}{(1+i)^t}}{\sum_{t=1}^{t=n} \frac{w_{dis}}{(1+i)^t}} \tag{17}$$

The CAPEX of the system is broken down into expenditure relating to the conversion of power (motor-generator & heat pump system) and expenditure for storage (storage tanks, storage medium etc.). The cost of the storage medium is 0.015 €/kWh which is insignificant compared to other components. The cost of latent heat storage medium has been found to be similar [39] and thus will not affect the overall LCOS.

Table 3
LCOS parameters.

CAPEX		OPEX		Discount	c_{el}	Lifetime
(€/kW)	(€/kWh)	(€/kW)	(€/kWh)	(%)	(€)	(years)
573	17	0.0026	11	0.08	0.03	20

The proposed PTES system is similar to the storage system on which Smallbone et al. [22] conducted their analysis. Both operate magnetite packed bed hot and cold storage tanks with a motor-generator connecting the compressor and expander on a single shaft. The pressure ratio of compressor and expander is the same, implying similar costs for CE and the pressurised hot and cold stores. Therefore, the costs used in the current model were based on the 'target system' pricing proposed by Smallbone et al. [22], with a system lifetime of $n = 20$ years and are shown in Table 3.

The economic benefit of arbitrage is beyond the scope of the current work. This omission is made with the assumption that a competitive system without arbitrage will only demonstrate improved benefits with its implementation.

4. Results & discussion

4.1. Working fluid and system performance with ideal thermal storage

While Air, Argon or other monatomic gasses are common in B-PTES cycles, fluids appropriate for this B-PTES cycle have been explored. Working fluids in the *CoolProp* library [27] have been assessed for thermodynamic, safety and environmental suitability.

123 working fluids were analysed using Eq. (2) to ensure a gaseous phase at the cycle extremes: state 2 ($P_2 = 10$ bar) & state 4 ($P_4 = 1$ bar) and that the highest temperature would not exceed material working limits suggested by Périlhon et al. [40] of $T_2 \leq 1073$ K. Carbon Dioxide, a working fluid common in Rankine and Transcritical PTES systems, is ruled out at this stage with a freezing temperature of 216 K. 97 other working fluids were also removed at the same stage due to their latent properties making them unsuitable for a Brayton cycle.

The remaining 25 working fluids were then scrutinised against the EU '*F gas*' regulations [41] of GWP < 150 and Ozone regulations [42] of ODP < 0.02. The final selection were trialled for flammability, economic viability and toxicity.

Argon (Ar), Helium (He), Oxygen (O_2), Nitrogen (N_2) & *Air* were identified as acceptable working fluids for a system working with a pressure ratio of ten.

4.1.1. Isentropic system performance

Eq. (4) demonstrates the reliance of the isentropic system performance on system temperatures, and pressure ratio, polytropic index, and isentropic efficiency of CE. Fig. 5 shows the relationship between η_{CE} and η_{rt} for the selected working fluids.

As the temperature ratio for a given pressure ratio is greater in monatomic fluids (*Ar* and *He*) than diatomic (O_2 and N_2) fluids, they are able to achieve higher η_{rt} for given system conditions. This advantage comes from the ratio of specific heats (adiabatic index), $\gamma^{monatomic} = 1.66$ compared to $\gamma^{diatomic} = 1.4$ demonstrated by Eq. (2). N_2 comprises 78% of Air with O_2 forming a further 20%, explaining why Air behaves like a diatomic gas. Monatomic gases were considered further in this study to maximise system efficiency.

4.1.2. Work flows in a B-PTES system

While Eq. (4) suggests that a system based on *Ar* or *He* would demonstrate the same performance, consideration of the energy and flow rate required to raise the temperature of the storage material highlights the differences between these fluids.

The specific heat capacity of *He* is ten times greater than that of *Ar* developing ten times more work across the CE devices as quantified

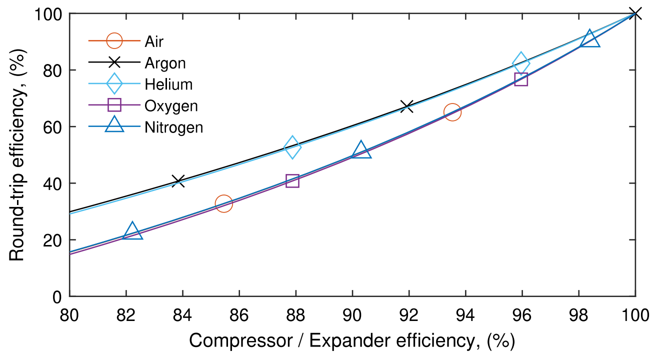

Fig. 5. Effect of η_{CE} on η_{rt} for selected B-PTES working fluids, with $PR = 10$.

Table 4
B-PTES system conditions for an isentropic system with ideal storage where $T_1 = T_3 = T_{amb}$.

P_{rated} (MW)	E_{store} (GJ)	PR	T_{amb} (K)	T_2 (K)	T_4 (K)	η_{CE}	η_{rt}
1	14	10	281	717	114	97.5	89.0

in Eq. (3). Fig. 6 shows the distribution of work in each process. Workflows have been calculated by the enthalpy difference between the states of each process. The difference between w_{TES} and w_{CE} can be accounted for by pressure ratio across the CE architecture giving rise to a greater enthalpy change than the isobaric TES.

For a given power input the required mass flow rate is $\dot{m} = P/w_C$. For the proposed system this ten fold scaling factor implied an infeasible $\dot{m}$ (very small) for a *He* system using common components and so *Ar* was selected as the working fluid. The potential to deploy ten times smaller PTES units using *He* as working fluid, each operating at a reduced power, is interesting and an analysis and costing of such a system could form the basis for further analysis.

For the system specified, the net charge work was $w_{chg} = 160$ kJ/kg and the initial mass flow rate for charge and discharge was 6.25 kg/s to meet the 1.0 MW desired power specification.

Within each analysis, $\dot{m}$ has been selected to ensure the most efficient model fills the specified four hour discharge period to allow comprehensive analysis of the trends of the results. Further work is required to identify the optimum absolute values for each investigation beyond the trends presented in this work.

4.1.3. System specification

The rated power, storage capacity, temperatures, CE isentropic efficiency and round trip efficiencies for the specified Argon PTES system with ideal thermal storage can be seen in Table 4.

4.2. Impact of practical TES

To assess the performance of the system with non-ideal storage the transient TES model has been deployed to analyse TES geometry and operation and predict the performance of additional latent storage.

Following the method in Section 3.3, the volume of the hot tank was found to be 21 m^3 and the volume of the cold tank was 46 m^3. This volume difference is due to the specific heat capacity difference of magnetite at high and low temperature, as well as the different ΔT applied to hot and cold stores. This further demonstrates the enhanced energy density of sensible storage in the hot store is more demanding in comparison with the cold store.

4.2.1. Geometric analysis

The volume to area ratio has been investigated by varying the length of the hot and cold storage tanks. Tank length and cross-sectional area were limited to a range of feasible physical geometries with the length of the hot store: 3 m < L_{hot} < 6 m (7 m^2 > A_{hot} > 3.5 m^2) and the cold store: 2 m < L_{cold} < 10 m (23 m^2 > A_{cold} > 4.6 m^2). By decreasing the area beyond a certain limit, boundary layer effects become significant, and pressure losses increase. Area optimisation was not the main focus of the research, justifying the use of representative lengths as selected with the objective optimum geometry of storage tanks an area for further work.

Fig. 7 shows the effect of TES length on η_{rt}. Varying the aspect ratio was found to have a large effect on system performance with trends suggesting that longer, thinner tanks improve system η_{rt}. The maximum reported η_{rt} from this analysis was 52.38%.

With all 20 permutations of tank length, the system discharge power demonstrated a region of maximum value, P_{peak}, lasting for a period of t_{pm} before falling to 0 kW in a 'power front'. Decreasing the area of the storage tanks was found to extend t_{pm} and flattened the power front. Elongating the hot store caused the time that T_{exit} (the exit gas temperature) was maintained at the storage temperature to increase from 0.25 h to 1.5 h. In the cold store, this period increased from 0 h to 1.4 h. The speed with which the layers of storage discharged their energy decreased with decreasing tank area, 'steepening' the power front. The benefit of extending t_{pm} can be seen in Fig. 7, halving A_{hot} resulted in an increase of 22% in η_{rt} for each cold store, while scaling A_{cold} to 20% of its original value gave a 5% improvement.

4.2.2. Segmentation operation

Segmentation has been investigated in an attempt to extend t_{pm} and steepen the power front.

In discharge process, the fraction of the temperature of the final active solid layer to the storage temperature is allowed to fall before the next segment is activated, which has been varied from 90% to 40% in a step of 10%. Segmentation demonstrated a linear variation in η_{rt} between the operational extremes. The distributions of P_{dis} and $T_{s,hot}$ for the extreme cases are shown in Fig. 8 to highlight the effect of segmentation on P_{peak} and t_{pm}. Each of the 20 segments of the hot TES are represented as un-marked coloured lines on the temperature plots.

Allowing the TES segments to discharge sequentially rather than draining energy from all of the segments at once increases t_{pm} from 1.2 h in an unsegmented storage to 1.7 h in a storage operating with a temperature fraction of 90%. In addition, the reduction in the active length of TES reduces pressure losses, allowing the energy of the gas to drive the CE rather than being lost in contact forces.

A temperature fraction of 40% allows the outlet gas temperature to fall to 350 °C in the hot TES and −60 °C in the cold TES before opening the next segment layer. This reduces the maximum instantaneous P_{dis} to between 740 kW and 640 kW as the segment discharges. Conversely, maintaining the final active solid temperature within 90% of storage temperature ($T_{2,4}$) reduces the power variation to 20 kW (from 840–820 kW) during the maximum power region.

Smaller temperature fractions demonstrate longer t_{pm} at the cost of P_{peak}. This illustrates the greater dependency of η_{rt} on the magnitude of peak power than its duration as found in Section 4.2.1. Segmented storage improves η_{rt} from about 53% (no segmentation in Section 4.2.1) to 55%. The storage operation selected for the study with additional latent storage in the next section was a 90% temperature fraction.

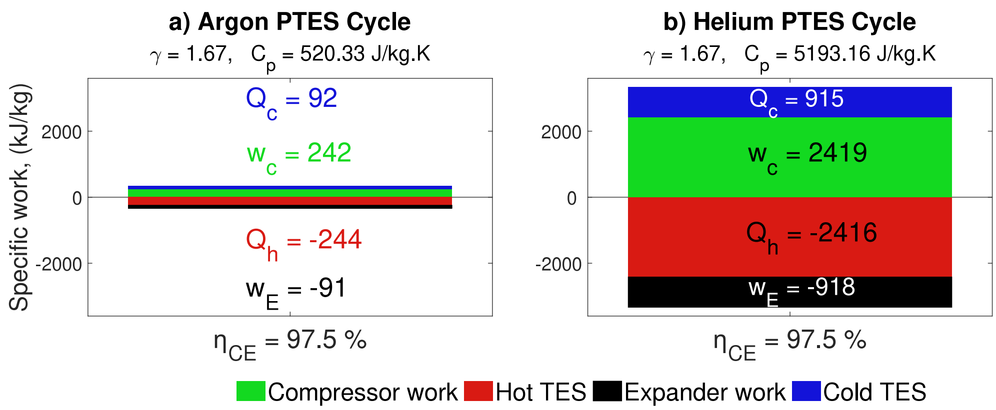

Fig. 6. Workflows in B-PTES cycles using a reciprocating CE architecture.

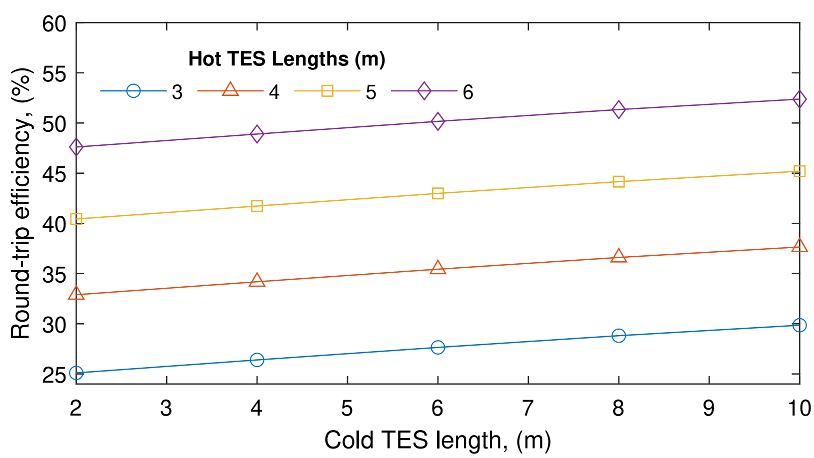

Fig. 7. Assessment of the effect of tank aspect ratio on η_{rt}.

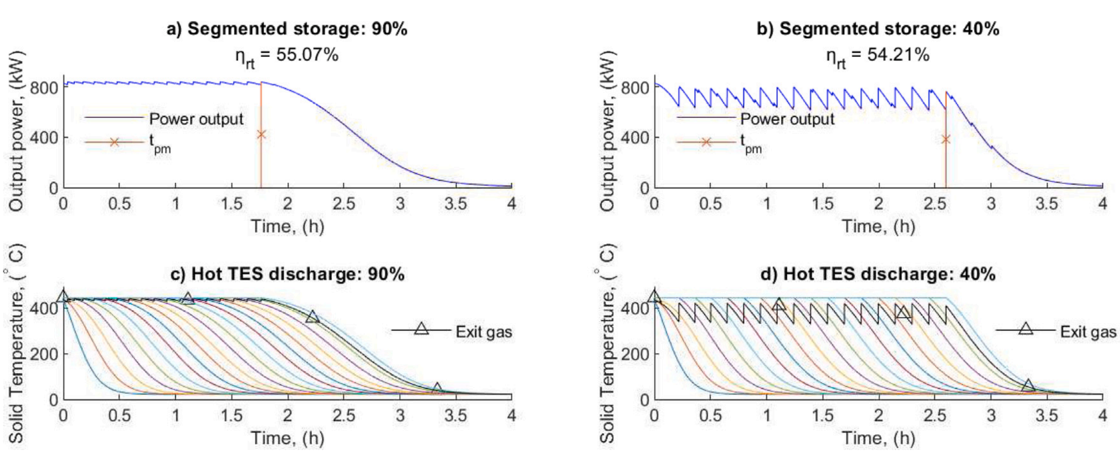

Fig. 8. System output power and solid temperature profiles of hot store. Output power is shown for the extremes of temperature fraction in (a) and (b). The variation of hot TES solid and gas temperature at exit (T_{exit}) is also presented for the extreme cases in (c) and (d). t_{pm} for a 90% temperature fraction: 1.7 h & t_{pm} for 40%: 2.6 h.

4.3. Additional latent storage

The main focus of this section was analysis of the novel addition of encapsulated PCMs and their effect on η_{rt}. For this analysis, the volumes of the tanks were increased and PCMs added downstream of the main storage section; the length of each store was increased by 50%. This quantity of additional latent storage was selected to allow detailed analysis of the properties of the discharge phase. Further analysis into the quantity of latent storage is required to identify an optimum value.

The PCMs detailed in Section 3.5 have been combined and permutated to assess the effect of melting temperature and latent heat on t_{pm} and η_{rt}. In the energy discharge stage, phase change begins as the main T_{exit} from sensible storage cools below T_{melt}. As the layers of latent storage change phase, the temperature of gas exiting the TES remains constant at T_{melt} until the PCM has transferred all of its latent heat to the gas. The duration of this phase change is a function of latent heat of PCM, ΔH, and the rate of heat transfer. The heat transfer is proportional to the gas–solid temperature difference, implying that the rate at which the latent heat consumption is dependent on melting temperature, heat

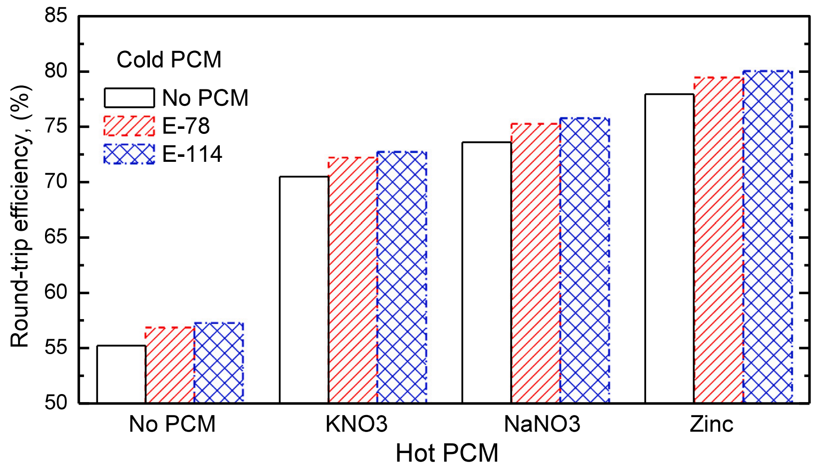

Fig. 9. Effect of permutations of additional latent storage on η_{rt}.

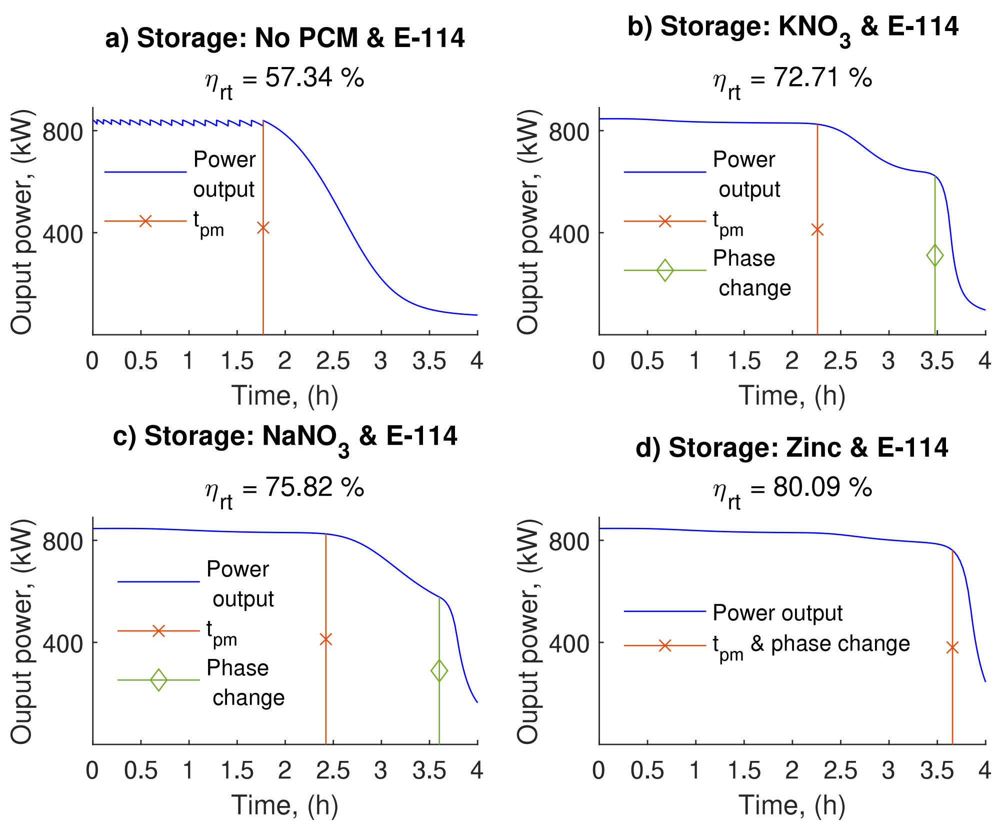

Fig. 10. Output power curves for permutations of hot PCM and *E-114*. t_{pm} for no hot PCM: 2.6 h, KNO_3: 2.3 h, $NaNO_3$: 2.4 h & *Zinc* 3.7 h.

transfer area and thermal conductivity of PCM as indicated by Eq. (5). The relative performance of the permutations of PCM are shown in Fig. 9. The combination of *Zinc* and *E-114* demonstrated the best system performance with a η_{rt} of 80%. The relative effect of each permutation of hot PCM in combination with *E-114* can be seen in Fig. 10.

Both of the cold PCMs slowed the increase in temperature of gas exiting cold TES; the extra mass of cold storage increased the duration of minimum gas outlet temperature from cold storage. However, T_{exit} from sensible cold storage and T_{melt} of cold PCM maintained an insufficient difference to produce a noticeable effect of cold PCMs on system performance. This is seen by the absence of a kink at three hours in Fig. 10(a–d) when the outlet gas (cold store) temperature reaches the melting temperature of *E-114* (the kink in the figure is mainly the results of using hot PCMs). And neither cold PCM fully discharges by the termination of the simulation at four hours. As indicated by their 1% respective increase on η_{rt} this has little effect on overall performance with using *E-78* developing only 40 kW more than the base case in four hours and *E-114* developing only 50 kW more.

As the hot sensible storage T_{exit} decays, as shown in Fig. 10, the system power output with additional $NaNO_3$ and KNO_3 storage drops to a level proportional to the temperature difference between melting temperature of PCM and gas outlet temperature from hot sensible storage (560 kW: $NaNO_3$ & 630 kW: KNO_3 at the end of phase change as indicated in the figure by diamond green line). While the phase change temperature of $NaNO_3$ is lower than KNO_3, it maintains t_{pm} for a greater duration and demonstrates slower heat transfer, thus offering a 3% improvement in η_{rt}.

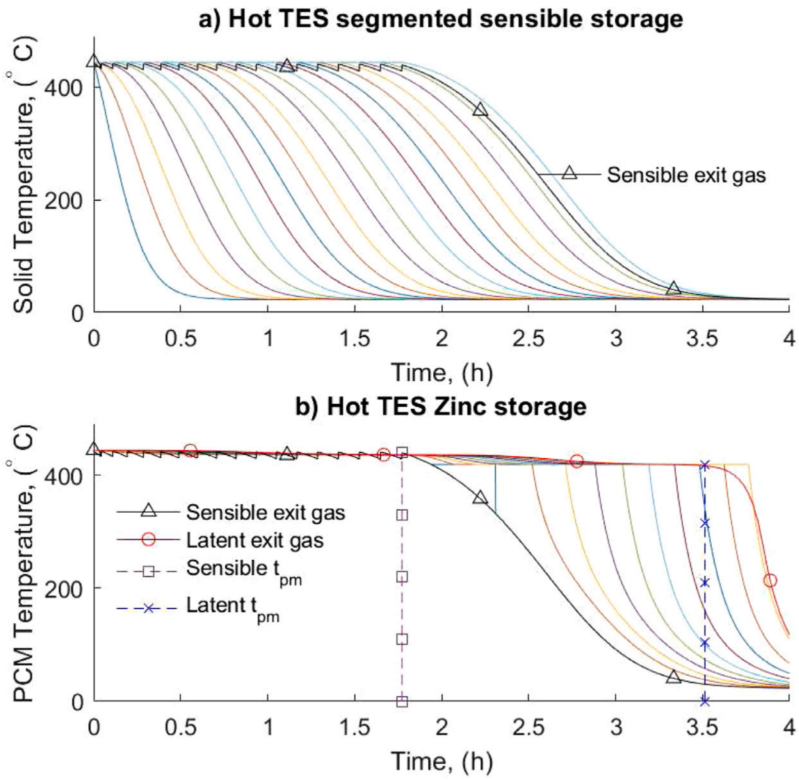

Fig. 11. Temperature variation of the sensible and latent (Zinc) TES during discharge. Temperatures of the gas exiting each store (T_{exit}) are also shown. Sensible t_{pm}: 1.8 h & Latent t_{pm} = 3.5 h.

Fig. 10(d) shows the improved power front that *Zinc* provides in comparison with magnetite shown in 10(a). The longer plateau caused by phase change indicates more complete utilisation of the energy store by using additional *Zinc* than using magnetite only and other hot PCMs. That is the key to achieve high round-trip efficiency. Fig. 11 further demonstrates the benefit of additional latent *Zinc* storage in extending t_{pm}. The decrease in T_{exit} from the sensible section begins after 1.8 h and decays to ambient over 1.5 h. With the latent storage, phase change continues for an additional 2 h after the temperature of the final layers of sensible storage have begun to cool. This inflates the temperature of the gas entering the CE devices compared to a system with only sensible storage, thus developing a greater P_{dis}.

Considering the residual energy in the outlet gas at the end of the four-hour discharge process, Fig. 11(b) shows T_{exit} to still be around 100 °C; however, the wasted heat is negligible as this temperature is only in the last layer. All of the sensible storage and 60% of latent TES layers are fully discharged, demonstrating the benefit to the round-trip efficiency.

Predicting PCM performance in future systems and developing methods of optimising the volume of PCM required against cost are areas to be explored further. In addition, the minimum quantity of PCM required to fulfil a specific discharge profile and the optimisation of this quantity against $\dot{m}_{dis}$ need investigation. Furthermore, for systems with a long storage duration, T_{melt} must be suitably selected to be well below any temperature reached by self discharge and storage losses. For example, the temperature difference between T_2 and the phase change temperature for *Zinc* is only 27 °C and the storage temperature dropping below this could reduce the efficiency of the system. Specific analysis will be required in the implementation of individual PCMs with each system if they are to be commercially deployed in the future.

4.4. Levelised cost of storage

Comparison of the baseline case (with optimised storage tank cross-sectional area and segmentation) to the cost of storage utilising PCMs suggested a saving of 0.04 €/kWh. The effect of η_{rt} on LCOS component costs are shown in Fig. 12.

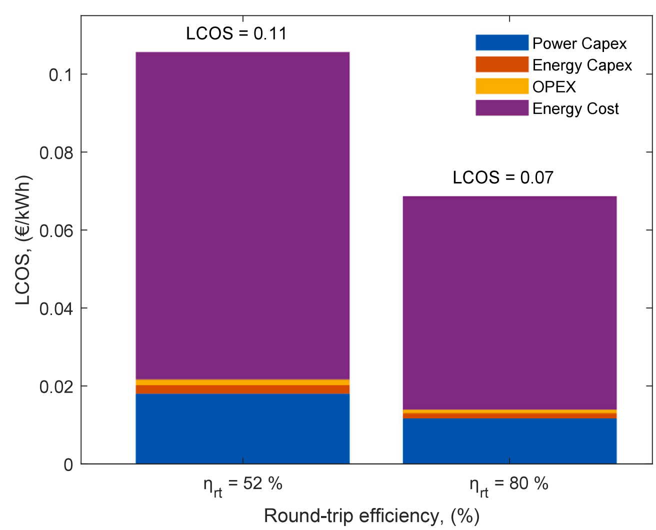

Fig. 12. LCOS for baseline case with sensible TES, η_{rt} = 52%, and a PTES system with additional latent storage, η_{rt} = 80%.

As noted by Smallbone et al. [22], the cost of electricity is shown to be the dominant system cost. Electricity comprises 0.08 €/kWh of the LCOS in the baseline case. Improving η_{rt} with additional latent storage reduces this to 0.05 €/kWh. With the current η_{rt} approaching the second law limit predicted by McTigue [11], developers will have to look for new ways to improve the economic viability of PTES systems. Integrating renewable energy sources such as wind farm could provide such an option. Using wind generated electricity, the operator avoids purchasing it to charge the system. As a unit of electricity is bought for a greater sum that it can be sold for, the operator saves money furthering the economic attractiveness of the scheme through the use of arbitrage [5,43].

However, it is noted that LCOS analyses should not be used to compare between PTES technologies, between storage methods [44]. Thus, it is the absolute LCOS value in comparison with PHS and battery which should be considered. The system identified in Section 4.2.2 (with segmented sensible heat storage) demonstrates comparable performance to PHS and better performance than all types of electric battery identified in [22]. The addition of latent storage further brings the system LCOS down, below the lower band of PHS and batteries, demonstrating the economic potential of a latent-hybrid system.

The marginal performance benefit gained by additional latent storage in the cold TES is found to have an affect of 0.0013 €/kWh on the system LCOS. Further detailed modelling is required to assess if this is economically worth-while.

5. Conclusion and future works

This study has found that the integration of additional latent storage into an Argon based Brayton PTES cycle can improve system performance, suggesting η_{rt} up to 80%. Such performance is close to the maximum suggested by McTigue [11].

As discharge time was constrained by renewable energy source and market conditions, the objective of this study was to maximise the duration of the high power region and decrease the size of the power front in CE device. This can be achieved by elongating the tanks and increasing the segmentation temperature ratio.

Additional latent storage was found to have a significant effect on the key features of the discharge phase. The involved latent storage maintained the temperature of the exit gas at high level for longer time, and led to a cliff-like drop of the temperature at final discharge stage. This allowed the storage to completely discharge and a greater proportion of the stored energy to be returned as useful work. Moreover, the addition of latent storage brings the LCOS below the value predicted for pumped hydro storage. In the future, practical experimentation is required for a deeper understanding of the actual effect of phase change materials on the thermal fronts, and transient analysis of the segmentation system and CE architecture must be incorporated into the TES models to estimate the absolute system performance.

While latent storage was found to extend t_{pm} in certain circumstances, use of a fully latent store is not predicted to be beneficial due to its lower specific heat and therefore lower total energy that can be stored in the packed bed. The optimum quantity of additional storage should form the basis of further work. Lack of data surrounding the transient properties of the PCMs is suggested to be a limitation of this study. However the model itself enjoys a high level of confidence due to previous experimental validation of similar systems. Further work would investigate the relative benefit of comparing additional sensible and latent storage which was omitted from this work.

The careful selection of $\dot{m}_{dis}$ is crucial to ensure the performance of the system. The rated power of the system affects $\dot{m}_{chg}$ and the size of the CE devices. Further investigation is needed to explore the implications of multi PTES systems for one renewable energy source field, e.g. a wind farm, or a single aggregated PTES for the whole site on system performance. Furthermore, it is suggested that reciprocating machines will be more efficient than turbomachinery only for systems with low power ratings (< 50 MW). Therefore, the specification of future systems has implications for CE architecture and overall system efficiency. It is recognised that use of the highly efficient reciprocating CE devices contributed to the high predicted efficiency of the system and other assumptions such as ideal electro-mechanical conversion are also likely to reduce the energy reclaimed in discharge in a real system.

CRediT authorship contribution statement

Max Albert: Software, Formal analysis, Writing – original draft. **Zhiwei Ma:** Conceptualization, Methodology, Writing – review & editing. **Huashan Bao:** Conceptualization, Investigation. **Anthony Paul Roskilly:** Conceptualization, Supervision.

Declaration of competing interest

The authors declare that they have no known competing financial interests or personal relationships that could have appeared to influence the work reported in this paper.

Acknowledgements

The authors gratefully acknowledge the support from the Solar S&HP project (EP/T023090/1) and DELTA PHI project (EP/T022981/1) funded by the UK Engineering and Physical Science Research Council. Data supporting this publication is openly available through Durham Research Online DATAsets Archive (DRO-DATA).

References

[1] UN General Assembly. Resolution 70/01, "Transforming our world: the 2030 agenda for sustainable development", A/RES/70/1. 2015.
[2] IEA. Tracking energy integration 2020: Energy storage. Paris: IEA.
[3] Gallo A, Simões-Moreira J, Costa H, Santos M, Moutinho dos Santos E. Energy storage in the energy transition context: A technology review. Renew Sustain Energy Rev 2016;65:800–22.
[4] Five steps to energy storage. World Energy Council; 2020.
[5] Dunbar A, Cradden L, Wallace R, Harrison G. Impact of wind power on arbitrage revenue for electricity storage. IET Gener Transm Distrib 2016;10(3):798–806.
[6] Beltran Hector, Harrison Sam, Egea-Àlvarez Agustí, Xu Lie. Techno-economic assessment of energy storage technologies for inertia response and frequency support from wind farms. Energies 2020;13(13):3421.
[7] Aneke Mathew, Wang Meihong. Energy storage technologies and real life applications–A state of the art review. Appl Energy 2016;179:350–77.
[8] https://www.maltainc.com/.
[9] Howes Jonathan. Concept and development of a pumped heat electricity storage device. Proc IEEE 2012;100(2):493–503.
[10] https://www.man-es.com/discover/a-tale-of-fire-and-ice.
[11] McTigue J. Analysis and optimisation of thermal energy storage (Ph.D. thesis), University of Cambridge; 2016.
[12] White A, Parks G, Markides CN. Thermodynamic analysis of pumped thermal electricity storage. Appl Therm Eng 2013;53(2):291–8.
[13] McTigue Joshua D, White Alexander J, Markides Christos N. Parametric studies and optimisation of pumped thermal electricity storage. Appl Energy 2015;137:800–11.
[14] Benato A. Performance and cost evaluation of an innovative Pumped Thermal Electricity Storage power system. Energy 2017;138:419–36.
[15] Benato Alberto, Stoppato Anna. Energy and cost analysis of a new packed bed pumped thermal electricity storage unit. J Energy Resour Technol 2018;140(2).
[16] Laughlin Robert B. Pumped thermal grid storage with heat exchange. J Renew Sustain Energy 2017;9(4):044103.
[17] White Alexander J. Loss analysis of thermal reservoirs for electrical energy storage schemes. Appl Energy 2011;88(11):4150–9.
[18] McTigue JD, White AJ. Segmented packed beds for improved thermal energy storage performance. IET Renew Power Gener 2016;10(10):1498–505.
[19] Farres-Antunez Pau, Xue Haobai, White Alexander J. Thermodynamic analysis and optimisation of a combined liquid air and pumped thermal energy storage cycle. J Energy Storage 2018;18:90–102.
[20] Howes J, Patent No:WO/2009/044139. Energy storage. 2009.
[21] Zanganeh Giw, Commerford Mark, Haselbacher Andreas, Pedretti Andrea, Steinfeld Aldo. Stabilization of the outflow temperature of a packed-bed thermal energy storage by combining rocks with phase change materials. Appl Therm Eng 2014;70(1):316–20.
[22] Smallbone A, Jülch V, Wardle R, Roskilly A. Levelised cost of storage for pumped heat energy storage in comparison with other energy storage technologies. Energy Convers Manage 2017;152:221–8.
[23] Oró E, Gil A, de Gracia A, Boer D, Cabeza L. Comparative life cycle assessment of thermal energy storage systems for solar power plants. Renew Energy 2012;44:166–73.
[24] Lazard's levelized cost of storage analysis - version 2.0. 2016.
[25] White A, McTigue J, Markides C. Wave propagation and thermodynamic losses in packed-bed thermal reservoirs for energy storage. Appl Energy 2014;130:648–57.

[26] Grosu Y, Faik A, Ortega-Fernández I, D'Aguanno B. Natural magnetite for thermal energy storage: Excellent thermophysical properties, reversible latent heat transition and controlled thermal conductivity. Solar Energy Mater Solar Cells 2017;161:170–6.

[27] Bell I, Wronski J, Quoilin S, Lemort V. Pure and pseudo-pure fluid thermophysical property evaluation and the open-source thermophysical property library CoolProp. Ind Eng Chem Res 2014;53(6):2498–508.

[28] Wang L, et al. Cyclic transient behavior of the joule–brayton based pumped heat electricity storage: Modeling and analysis. Renew Sustain Energy Rev 2019;111:523–34.

[29] Wakao N, Kaguei S, Funazkri T. Effect of fluid dispersion coefficients on particle-to-fluid heat transfer coefficients in packed beds. Chem Eng Sci 1979;34:325–36.

[30] Ergun S. Fluid flow through randomly packed columns and fluidized beds. Ind Eng Chem 1949;41(6):1179–84.

[31] Howes J, Hunt R. Improved heat storage apparatus. 2012, WO Patent: GB 2012071145.

[32] Zhao W, et al. Thermal energy storage using zinc as encapsulated phase change material. Thermodyn Sustain 2011;4.

[33] Ho Cho Yen, Powell Ralph Waterbury, Liley Peter E. Thermal conductivity of the elements: a comprehensive review. 1974.

[34] Alam T. Experimental investigation of encapsulated phase change materials for thermal energy storage (Ph.D. thesis), University of South Florida; 2015.

[35] Xiao X, Zhang P, Li M. Thermal characterization of nitrates and nitrates/expanded graphite mixture phase change materials for solar energy storage. Energy Convers Manage 2013;73:86–94.

[36] Nagasaka Yuji, Nagashima A. The thermal conductivity of molten NaNO 3 and KNO 3. Int J Thermophys 1991;12(5):769–81.

[37] PCM Products. Pcm solutions, ultra low eutectic pcms. 2021, https://www.pcmproducts.net/Phase-Change-Material-Solutions.htm [Accessed 22nd Feb 2021].

[38] Schoenung S. Characteristics and technologies for long vs. short term energy storage. Technical report, Sandia National Laboratories; 2001.

[39] Nieto-Maestre J, et al. Novel metallic alloys as phase change materials for heat storage in direct steam generation applications. AIP Conf Proc 2016;1734(1):050032.

[40] Périlhon C, Lacour S, Podevin P, Descombes G. Thermal electricity storage by a thermodynamic process: Study of temperature impact on the machines. Energy Procedia 2013;36:923–38.

[41] Regulation (EU) no 517/2014 of the European parliament and of the council. 2014.

[42] Regulation (EC) no 1005/2009 of the European parliament and of the council. 2009.

[43] Nord Pool: Data market. Market data: N2EX day ahead auction prices. 2020, https://www.nordpoolgroup.com/Market-data1/GB/Auction-prices/UK/Hourly/?view=table [Accessed 2nd Nov 2020].

[44] Aldersey-Williams J, Rubert T. Levelised cost of energy – a theoretical justification and critical assessment. Energy Policy 2019.